

# Geophysical Research Letters®

#### RESEARCH LETTER

10.1029/2021GL094443

#### **Key Points:**

- · Dispersion coefficient
- Convolutional neural network
- · Flow through porous media

#### Correspondence to:

M. Sahimi, moe@usc.edu

#### Citation:

Kamrava, S., Im, J., de Barros, F. P. J., & Sahimi, M. (2021). Estimating dispersion coefficient in flow through heterogeneous porous media by a deep convolutional neural network. *Geophysical Research Letters*, 48, e2021GL094443. https://doi.org/10.1029/2021GL094443

Received 24 MAY 2021 Accepted 16 JUL 2021

# Estimating Dispersion Coefficient in Flow Through Heterogeneous Porous Media by a Deep Convolutional Neural Network

Serveh Kamrava<sup>1</sup>, Jinwoo Im<sup>2</sup>, Felipe P. J. de Barros<sup>2</sup>, and Muhammad Sahimi<sup>1</sup>

<sup>1</sup>Mork Family Department of Chemical Engineering and Materials Science, University of Southern California, Los Angeles, CA, USA, <sup>2</sup>Sonny Astani Department of Civil and Environmental Engineering, University of Southern California, Los Angeles, CA, USA

**Abstract** Estimating the longitudinal dispersion coefficient  $D_L$  in flow through heterogeneous porous media is paramount to many problems in geological formations. Moreover, although it is well-known that  $D_L$  is sensitive to the morphology of such formations, it has been very difficult to establish a firm link between the two. We describe a novel deep convolutional neural network (DCNN) for estimating  $D_L$ . The inputs for training of the network are a large and diverse set of data consisting of three-dimensional images of porous media, as well as their porosity, and the associated  $D_L$  values computed by random-walk particle-tracking (RWPT) simulations. The trained network predicts  $D_L$  very rapidly, and its predictions are in excellent agreement with the data not used in the training. Thus, a combination of the DCNN and RWPT simulation provides a powerful tool for studying many flow-related phenomena in geological formations, and estimating their properties.

**Plain Language Summary** Measuring or computing the dispersion coefficient  $D_L$  in flow through porous media, a fundamental characteristic of transport in geological formations and risk analysis, is a time-consuming endeaver. Moreover, although  $D_L$  is sensitive to the morphology of a pore space, a direct link between the two has been missing. We proposed a deep convolutional neural network for predicting  $D_L$ , using 3D images of porous media and their porosities. The accuracy of the predictions for the actual data indicates that the ability of the network for estimating the important flow and transport properties of porous media for new input data. The present work was at the core scale, on the order of the physical sizes of the sandstones used in our study. The same approach may be used at the eld scale. In that case, one generates the input data by following the same procedure, except that the data should be generated for models in which the permeability and porosity of the formation vary spatially, and represent correlated fields. Work in this direction is in progress.

# 1. Introduction

A solute, brought into contact with a miscible solvent, diffuses into the latter and gradually develops a diffused mixed zone. Provided that there is no change in the volumes of the solute and solvent as they mix, the transport of the former is governed by the diffusion equation. If the solvent is flowing, one will also have convective mixing due to the fluctuations in the velocity field. The phenomenon is then referred to as hydrodynamic dispersion, or simply dispersion. If the mixing occurs in a porous medium, the velocity field is affected by its heterogeneity, which in turn influences the concentration profile in the mixed zone. Such heterogeneities often give rise to non-Fickian transport that are difficult to model. Dispersion is important to many processes of practical interest, including storage and sequestration of CO<sub>2</sub> in deep saline aquifers, enhanced recovery of oil by miscible displacement (Sahimi, 2011), seawater intrusion into aquifers, risk analysis related to spreading of industrial wastes, groundwater pollution (Bear & Cheng, 2010; Helmig, 1997), and operation of packed-bed reactors. Thus, dispersion has been investigated for decades by experimental, theoretical, and computer simulation studies (see Sahimi, 2011, for a comprehensive review). Dispersion in microscopically heterogeneous, but macroscopically homogeneous porous media has been examined by both experiments and computer simulations. In particular, beginning with the work of Sahimi and co-workers (Sahimi et al., 1983, Sahimi, Heiba et al., 1986; Sahimi, Hughes et al., 1986, Sahimi & Imdakm, 1988), pore networks have been used to study dispersion, which has continued up until recently

© 2021. American Geophysical Union. All Rights Reserved.

KAMRAVA ET AL. 1 of 7

(Bijeljic & Blunt, 2006; Bijeljic et al., 2004). Modeling of porous media by pore networks and similar models inherently involves simplification of the pore space morphology. Thus, other computational approaches, such as the lattice-Boltzmann simulation (Manz et al., 2004) in images of the pore space (Meakin & Tartakovsky, 2009; Maier et al., 2000) and numerical simulation of the Stokes flow in the images and superimposing diffusion on the flow field through particle tracking (Bijeljic et al., 2011, 2013; Mostaghimi et al., 2012) have also been used to study dispersion. Recent experimental studies of dispersion utilized imaging technologies, such as X-ray computed tomography and positron emission tomography (Hasan et al., 2020; Pini et al., 2016; Zahasky & Benson, 2018). Pore-scale imaging and modeling have also been used to study dispersion in fluid flow, both numerically and by computer simulation (Blunt et al., 2013; Manz et al., 2004; Zahasky & Benson, 2018).

As an alternative approach, random-walk particle-tracking (RWPT) simulation in the Cartesian coordinates has also been developed. Although the RWPT simulation is known to be computationally more expensive than pore-network models, its computational burden was reduced considerably by the advent of a massively parallel computational strategy (Meakin & Tartakovsky, 2009). In this context, an open source for RWPT simulation, dubbed PAR<sup>2</sup>, was proposed by Rizzo et al. (2019) that utilizes graphics processing units (GPUs), and was employed to study transport of solutes at field scale (Rizzo & de Barros, 2017; Rizzo et al., 2019).

A most important characteristic of dispersion processes is the longitudinal dispersion coefficient  $D_L$ , which is a measure of the speed by which the solute spreads in the pore space in the direction of macroscopic flow. Its estimation by the aforementioned computational methods is, however, quite time consuming. Given the significance of dispersion to many phenomena in geological formations, developing a rapid and accurate method for estimating  $D_L$  is paramount. In this Letter, we propose a novel approach for computing  $D_L$  based on a combination of the RWPT simulation and a machine-learning (ML) algorithm, with the latter having been shown to be an efficient alternative for computating many properties of complex systems.

Deep-learning (DL) methods (LeCun et al., 2015; Schmidhuber, 2014), such as deep convolutional neural networks (DCNNs), have been developed to overcome the shortcomings of the conventional ML methods in processing complex and large datasets. The most common category of the DL methods is supervised learning methods in which the input data have labels, and the DCNN is utilized for identifying the nonlinear relation between the input data and their labels, that is, the calculated data. Such algorithms are commonly used for regression or classification purposes. In the former case, an image is used for training of the network, which then produces the output. The predicted output at the beginning of training is most likely far from the actual data, the so-called ground truth. Therefore, the DCNN calculates a loss or cost function, the sum of the squares of the differences between the predicted quantities and the data, and minimizes it through calculating optimal values of a number of adjustable parameters. After the training, the DCNN with the optimal parameters is tested with a new set of data. If successful, the network generalizes the ability of the DCNN for making predictions for new data (see Tahmasebi et al., 2020, for a comprehensive review). The approach has been used to link the morphology of a porous medium to its permeability (Kamrava et al., 2020), diffusivity (Wu et al., 2019), and other properties (Algahtani et al., 2020; Graczyk & Matyka, 2020). We describe, for the first time, a DCNN for predicting the longitudinal dispersion coefficient  $D_L$  in flow through disordered porous media.

The rest of the paper is organized as follows. In the next section, we describe the methodology, and the details of flow and the RWPT simulations, through which we generated the data for training the DCNN. Next, the structure of the network and the computational procedure are explained. The results using the trained DCNN are then presented. The key outcomes of the paper are summarized in the last section.

# 2. The Methodology

We first describe PAR<sup>2</sup>, the algorithm used for generating the data needed for the DCNN, after which we explain the DCNN itself.

KAMRAVA ET AL. 2 of 7

19448007, 2021, 18, Downloaded from https://agupubs.onlinelibrary.wiley.com/doi/10.1029/2021GL094443 by Pejman Tahmasebi , Wiley Online Library on [02/01/2023]. Sec

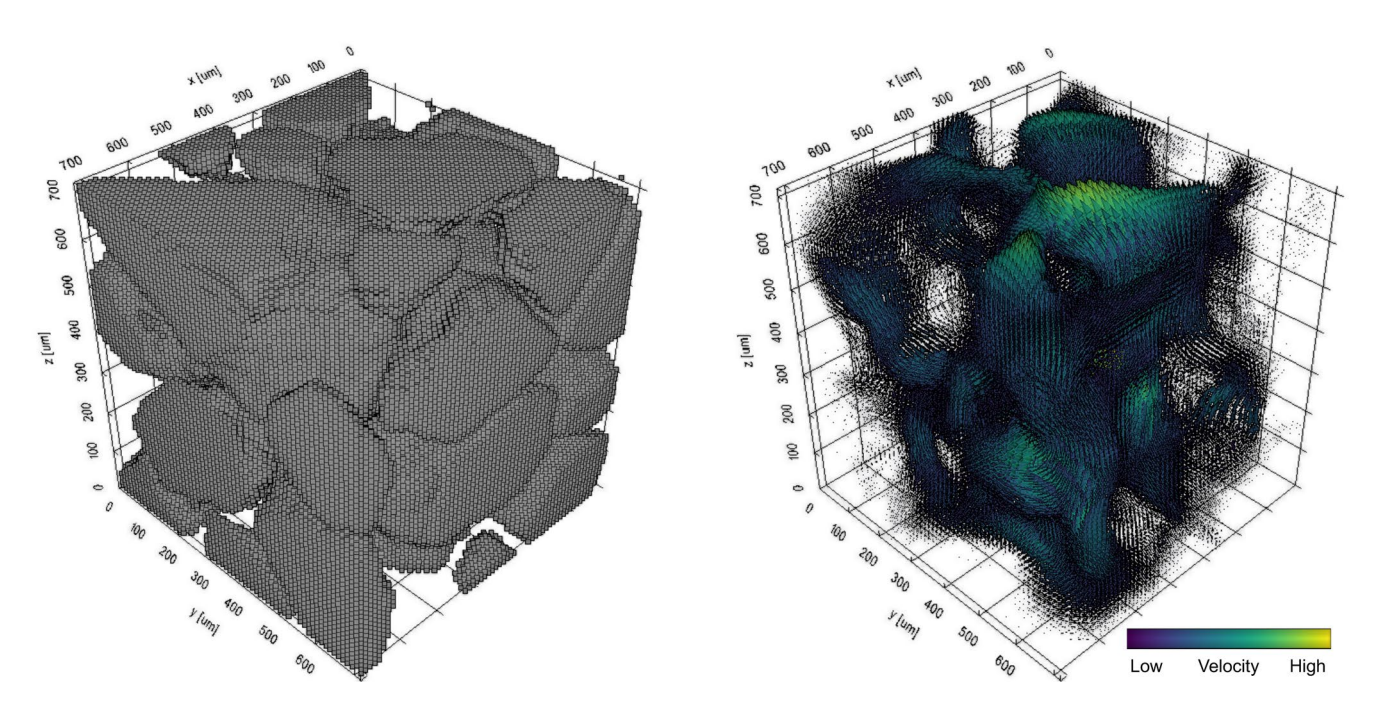


Figure 1. An example of a pore space (left) and the advective velocity field used in the random-walk particle-tracking simulation with the modified PAR<sup>2</sup>.

### 2.1. Random-Walk Particle Tracking

The original PAR<sup>2</sup> algorithm was designed for solute transport in a given velocity field with non-periodic boundary conditions (Rizzo et al., 2019). Thus, two changes were made for implementing it in a pore-scale domain. First, to ensure that the particles pass through a large enough pore space and yield representative dispersion coefficients, periodic boundary conditions (PBCs) were imposed in all three directions. Second, with the PBCs each time the particles exit from an external surface of the pore space, they should be put back into the pore space at the exact location on the opposite surface. However, doing so may cause the particles to get trapped in the solid space, since the pore and solid geometries at one boundary of the domain do not necessarily match those at the opposite boundary. To address this issue, we relocated the particles that exited from one external surface of the pore space to the nearest pore on the opposite surface, if there was no exact matching.

The trajectory of solute particle *i* is computed using the Ito—Taylor integration scheme (Risken, 1996):

$$\mathbf{X}_{i}(t + \Delta t) = \mathbf{X}_{i}(t) + \mathbf{A}[\mathbf{X}_{i}(t)]\Delta t + \mathbf{B}[\mathbf{X}_{i}(t)] \cdot \boldsymbol{\xi}(t)\sqrt{\Delta t}, \tag{1}$$

where  $\xi$  is a normally distributed random variable with zero mean and unit standard deviation,  $\Delta t$  is the time step, and the drift vector **A** and the displacement matrix **B** are defined by,

$$\mathbf{A}(\mathbf{x}) = \mathbf{u}(\mathbf{x}) + \nabla \cdot \mathbf{D}(\mathbf{x}) + \frac{1}{\phi(\mathbf{x})} \mathbf{D}(\mathbf{x}) \cdot \nabla \phi(\mathbf{x})$$
 (2)

$$2\mathbf{D}(\mathbf{x}) = \mathbf{B}(\mathbf{x}) \cdot \mathbf{B}(\mathbf{x})^{\mathrm{T}} \tag{3}$$

where **D** is the local dispersion tensor (Bear & Cheng, 2010), **u** is the velocity field,  $\phi$  is the effective porosity, and T denotes the transpose operation. We consider a 3D system, so that  $\mathbf{x} = (x, y, z)$ . In our analysis convection and diffusion in the pore space are both included (LaBolle et al., 1996; Salamon et al., 2006). The input for the PAR<sup>2</sup> are the fluid velocity field throughout the pore space; see Figure 1.

Dispersion simulations were carried out for 900 velocity fields, computed for 900 distinct 3D cores with dimensions  $64\Delta x \times 64\Delta y \times 64\Delta z$ , with  $\Delta x = \Delta y = \Delta z = 11.2 \,\mu\text{m}$ . Use of larger samples is, of course, possible, but that would increase the computational time significantly. On the other hand, very small images would not represent the heterogeneity of the medium. Preliminary simulations with various image sizes indicated that the selected size is representative. The molecular diffusivity was  $D_m = 10^{-9} \, \text{m}^2/\text{s}$ . The Péclet number Pe was computed by (Mostaghimi et al., 2012), Pe =  $u_a L/D_m$ , where  $u_a$  is the average velocity defined by,

KAMRAVA ET AL. 3 of 7

 $u_a = Q/(A\phi)$ , where Q is the volume flow rate in the pore space, A is the area perpendicular to the macroscopic flow direction, and L is the characteristic length scale. A typical grain size of sandstones was used for L, that is,  $L = 150 \,\mu\text{m}$ .

The average Pe over all 900 cores was  $10^3$ . In the RWPT simulation, 30,000 particles were randomly initialized in each pore space at one boundary of the domain. A dimensionless time  $\tau$  was defined by,  $\tau = t/t_c = t/(L/\overline{u}_a)$ , where  $t_c$  is the characteristic advective time which we took it to be  $2 \times 10^{-2}$ s, and  $\overline{u}_a$  is the ensemble mean of all the average velocities. The total simulation time T was set to  $2 \times 10^3 \tau$  with the time step  $\Delta t = 1 \times 10^{-3} \tau$ , so determined to restrict the movement of particles at one time step to one voxel.

The longitudinal dispersion coefficient  $D_L$  was computed for all the realizations by

$$D_L = \frac{1}{2} \frac{d\sigma_x^2}{dt},\tag{4}$$

where  $\sigma_x^2$  is the longitudinal variance of the particle displacement.

$$\sigma_x^2 = \left\langle \left[ x_i(t) - \langle x_i(t) \rangle \right]^2 \right\rangle \tag{5}$$

with  $x_i(t)$  being the displacement of the particle i (i = 1, 2, ..., 30000) in the longitudinal direction.

The results for  $D_L$  computed by PAR<sup>2</sup> had mean and standard deviations, respectively, of  $5 \times 10^{-6}$  and  $2 \times 10^{-5}$  m<sup>2</sup>/s. The mean  $D_L$  is of the same order of magnitude as that of the previous numerical and experimental data (Bijeljic & Blunt, 2006; Bijeljic et al., 2004; Pini et al., 2016; Sahimi, 2011; Zahasky & Benson, 2018). In particular, Sahimi (2011) presented the ratio  $D_L/D_m$  as a function of Pe for a large collection of data. His plot yields  $D_L = 10^{-6}$  m<sup>2</sup>/s for Pe =  $10^3$ , consistent with our mean value of  $D_L$ .

#### 2.2. The Deep-Learning Algorithm

The success of DL methods is dependent upon the availability of a large data set. Other factors contributing to the success include progress in the learning methods, as well as efficiency of the computations with GPUs (Shen et al., 2017). The DCNN used in this study consists of convolutional, batch normalization, activation, pooling, and fully connected layers (See Tahmasebi et al., 2020 for extensive discussions of the terminology).

The convolutional layer uses learnable kernels to identify the local features at various locations in the input data, and to construct the feature maps. The extracted feature maps are the essential information relating the input data and the output, after which a nonlinear activation function is applied. In the present study we used the rectified linear unit defined by,  $A(x) = \max(0, x)$ , which eliminates all the negative values since A(x) = 0 if x < 0 and, therefore, adds a small degree of nonlinearity to the convolved feature map, hence allowing the network to learn more about the input data. The functions acting on the 3D input data are represented by

$$f_{ijk}^{l} = \mathcal{A}\left(\sum_{i,j,k=1}^{M} f_{ijk}^{l-1} w_{ijk}^{l} + b_{l}\right),$$
 (6)

where  $f_{ijk}^l$  is the output of layer l,  $w_{ijk}^l$  is the learnable kernels applied to layer l, and  $b_l$  is the bias.

After the convolutional and activation layers comes pooling, which downsamples the feature maps of the previous convolutional layers and makes the network translationally invariant. We used a pooling layer that computes the average value for each path on the feature map (Kamrava et al., 2020). The output of the last pooling layer is then converted to a 1**D** vector, after which regression is carried out. To minimize the loss or cost function and determine the optimal values of the learnable parameters—the weights and biases—we used Adam optimization algorithm (Kingma & Ba, 2014). In this method the first and second moments of the gradient estimates of the learnable parameters are used for determining their learning rates. The nth moment of a learnable variable v is defined by,  $m_n = \mathcal{E}(v^n)$ , where  $\mathcal{E}$  denotes the expected value. To estimate the moments, the exponentially moving averages of the gradient and squared gradient at epoch t, given by,

$$m_1(t) = \beta_1 m_1(t-1) + (1-\beta_1)g(t), \tag{7}$$

$$m_2(t) = \beta_2 m_2(t-1) + (1-\beta_2)g^2(t), \tag{8}$$

were used, where  $\beta_1$  and  $\beta_2$  are hyperparameters for controlling the decay rates of the moving averages, and g is the gradient on the mini-batch that is being studied. Trial and error were used for setting the

KAMRAVA ET AL. 4 of 7

elibrary.wiley.com/doi/10.1029/2021GL094443 by Pejman Tahmasebi

Wiley Online Library on [02/01/2023]. See,

Figure 2. Schematic of the convolutional neural network.

hyperparameters. For example, we initially worked with five sets of convolution, activation, and pooling layers. Then, we varied the number of layers to understand its effect on the predictions. The initial values of  $\beta_1$ ,  $\beta_2$ , V and W are set to 0.9, 0.999, zero and zero, respectively. The DCNN contained 21 layers, eight convolutional layers with various number of filters, each of which was followed by a batch normalization, an activation and a pooling layer, except for the last layer that was fully connected one.

# 3. The Data and Computational Procedure

The data used for the training and testing included large 3D images of two porous media, the Berea, and Mt. Simon sandstone (Kohanpour et al., 2020; Tahmasebi et al., 2017) with porosities, respectively, of 0.196 and 0.25. The Berea sandstone (Raeini et al., 2014; Valvatne & Blunt, 2004) has a physical volume of 2.13 $^3$  mm $^3$ , and has used in many studies of flow and transport in porous media as a testing ground. The Mt. Simon sandstone, with a physical size of 3.36 $^3$  mm $^3$ , was taken at a depth of 6,700 feet in verification well number two of a study site in Decatur, Illinois, where Illinois State Geological Survey carried out a pilot injection to study the feasibility of full-scale  $CO_2$  sequestration. We extracted 900 3D images of size  $64 \times 64 \times 64$  voxels, with the size of the voxels being  $11.2^3$  µm $^3$ . 85 percent of the data were used for the training, and the rest for testing the accuracy of the DCNN. About 17 percent of the training data was used as validation data to ensure the trained network can handle unseen information. The training of the network took about two GPU hours using NVIDIA Tesla V100.

As the first step the pressure and velocity fields were computed by solving the Stokes' equations in the images. The results were then used as the input to the PAR<sup>2</sup> algorithm for computing the dispersion coefficients, which were then used for the training, validation and testing of the DCNN. We also supplied the porosity

data to the network as one of the important physical features. A Schematic of the network is shown in Figure 2.

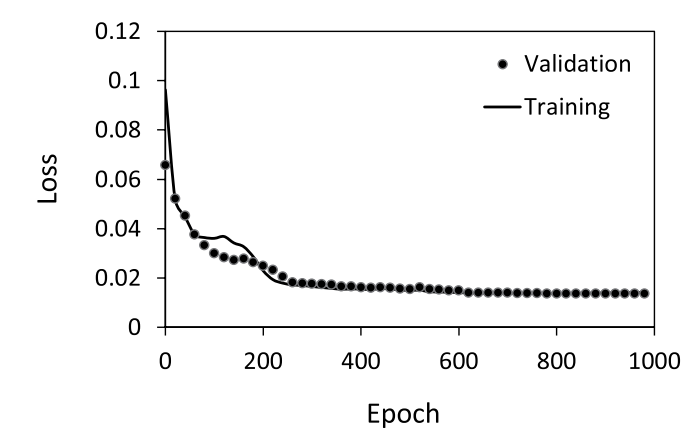


Figure 3. Loss function for training the convolutional neural network.

#### 4. Results

Figure 3 presents the decay of the loss function during the training. Its value is large at the beginning, being slightly larger for the validation data. But as the training continues, the loss functions for both validation and training decrease, meeting at a plateau.

After the training, the accuracy of the DCNN was checked with the testing data. Figure 4 demonstrates the capability of the network for predicting the dispersion coefficient  $D_L$ , based on the 3D images of the porous media and their porosity, for the the data that the DCNN had not used during its training. The dispersion coefficients are normalized between 0 and 1 by,  $\left(D_L - D_L^m\right) / \left(D_L^M - D_L^m\right)$ , where superscripts m and M denote the minimum and maximum values. The correlation coefficient between

KAMRAVA ET AL. 5 of 7

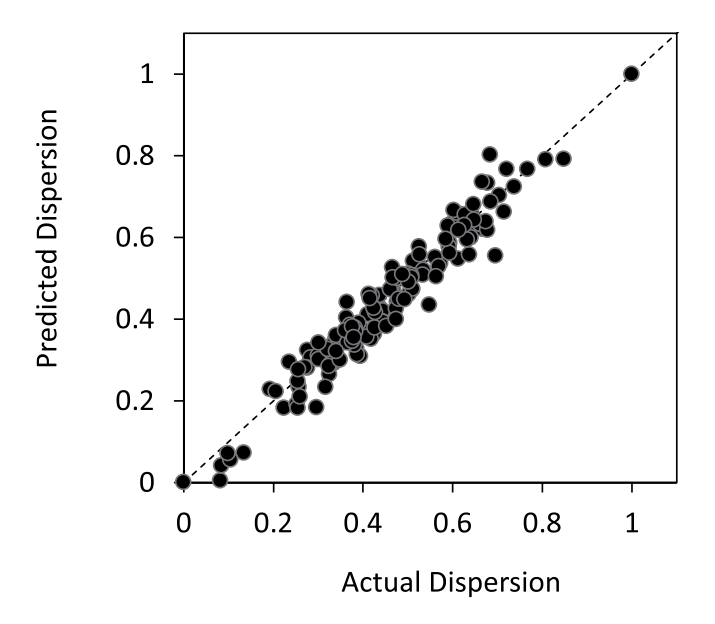


**Figure 4.** Predicted dispersion coefficients versus the actual data during testing of the deep convolutional neural network.

the predictions and the data is 0.94, indicating the high accuracy of the DCNN. Thus, the DCNN may be used readily with new images without carrying out any new simulations.

Note that for small values of  $D_L$  the predictions underestimate the corresponding actual values. For example, the first cluster of points in Figure 4 appear to be below the diagonal line, while other predictions for larger  $D_L$  are almost evenly distributed on both side of the diagonal. This is simply due to smaller number of data points for such  $D_L$  values.

One point is worth emphasizing. If we train the DCNN with the 3D images, but without utilizing explicitly the porosities of the samples as independent input data, the predictions will not be as accurate as those presented in Figure 4. This identifies porosity as a key factor in determining the dispersion coefficient.

# 5. Summary

Measuring or computing the dispersion coefficient  $D_L$  in flow through porous media, a fundamental characteristic of transport in geological formations and risk analysis, is a time-consuming endeavor. Moreover, although  $D_L$  is sensitive to the morphology of a pore space, a direct link between the two has been missing. We proposed a deep convolutional neural network for predicting  $D_L$ , using 3D images of porous media and

their porosities. The accuracy of the predictions for the actual data indicates that the ability of the network for estimating the important flow and transport properties of porous media for new input data.

The present work was at the core scale, on the order of the physical sizes of the sandstones used in our study. The same approach may be used at the field scale. In that case, one generates the input data by following the same procedure, except that the data should be generated for models in which the permeability and porosity of the formation vary spatially, and represent correlated fields. Work in this direction is in progress.

# **Data Availability Statement**

Data showing morphology of porous media samples used for training and testing the network is archived at https://zenodo.org/record/5120874#.YPilQuhKiUk.

#### Acknowledgments

Any related materials can be obtained from M. S. (moe@usc.edu).

# References

Algahtani, N., Alzubaidi, F., Armstrong, R. T., Swietojanski, P., & Mostaghimi, P. (2020). Machine learning for predicting properties of porous media from 2d X-ray images. *Journal of Petroleum Science and Engineering*, 184, 106514.

Bear, J., & Cheng, A. H.-D. (2010). Modeling groundwater flow and contaminant transport. Springer. https://www.springer.com/gp/book/9781402066818

Bijeljic, B., & Blunt, M. J. (2006). Pore-scale modeling and continuous time random walk analysis of dispersion in porous media. *Water Resources Research*, 42, W01202. https://doi.org/10.1029/2005wr004578

Bijeljic, B., Mostaghimi, P., & Blunt, M. J. (2011). Signature of non-Fickian solute transport in complex heterogeneous porous media. *Physical Review Letters*, 107, 204502. https://doi.org/10.1103/physrevlett.107.204502

Bijeljic, B., Muggeridge, A. H., & Blunt, M. J. (2004). Pore-scale modeling of longitudinal dispersion. Water Resources Research, 40, W11501. https://doi.org/10.1029/2004wr003567

Bijeljic, B., Raeini, A., Mostaghimi, P., & Blunt, M. J. (2013). Predictions of non-Fickian solute transport in different classes of porous media using direct simulation on pore-scale images. *Physical Review E, 87*, 013011. https://doi.org/10.1103/physreve.87.013011

Blunt, M. J., Bijeljic, B., Dong, H., Gharbi, O., Iglauer, S., Mostaghimi, P., et al. (2013). Pore-scale imaging and modelling. *Advances in Water Resources*, 51, 197–216. https://doi.org/10.1016/j.advwatres.2012.03.003

Graczyk, K. M., & Matyka, M. (2020). Predicting porosity, permeability, and tortuosity of porous media from images by deep learning. Scientific Reports, 10, 21488. https://doi.org/10.1038/s41598-020-78415-x

Hasan, S., Niasar, V. J., Karadimitriou, N. K., Godinho, J. R. A., Vo, N. T., An, S., et al. (2020). Direct characterization of solute transport in unsaturated porous media using fast X-ray synchrotron microtomography. *Proceedings of the National Academy of Sciences, USA*, 117, 23443–23449. https://doi.org/10.1073/pnas.2011716117

Helmig, R. (1997). Multiphase flow and transport processes in the subsurface. Springer. https://www.springer.com/gp/book/9783642645457

KAMRAVA ET AL. 6 of 7

- Kamrava, S., Tahmasebi, P., & Sahimi, M. (2020). Linking morphology of porous media to their macroscopic permeability by deep learning. Transport in Porous Media, 131, 427–448. https://doi.org/10.1007/s11242-019-01352-5
- Kingma, D. P., & Ba, J. (2014). A method for stochastic optimization. In: Proceedings of the 3rd International Conference on Learning Representations. ICLR, San Diego, CA. arXiv:1412.6980v9 [cs.L.G] 2017.
- Kohanpur, A. H., Rahromostaqim, M., Valocchi, A. J., & Sahimi, M. (2020). Two-phase flow of-brine in a heterogeneous sandstone: Characterization of the rock and comparison of the lattice-Boltzmann, pore-network, and direct numerical simulation methods. *Advances in Water Resources*, 135(1), 1–11. https://doi.org/10.1016/j.advwatres.2019.103469
- LaBolle, E. M., Fogg, G. E., & Tompson, A. F. (1996). Random-walk simulation of transport in heterogeneous porous media: Local mass-conservation problem and implementation methods. *Water Resources Research*, 32, 583–593. https://doi.org/10.1029/95wr03528 Lecun, Y., Bengio, Y., & Hinton, G. (2015). Deep learning. *Nature*, 521, 436–444. https://doi.org/10.1038/nature14539
- Maier, R. S., Kroll, D. M., Bernard, R. S., Howington, S. E., Peters, J. F., & Davis, H. T. (2000). Pore-scale simulation of dispersion. Physics of Fluids, 12, 2065–2079. https://doi.org/10.1063/1.870452
- Manz, B., Gladden, L. F., & Warren, P. B. (2004). Flow and dispersion in porous media: Lattice-Boltzmann and NMR studies. *AIChE Journal*, 45, 1845–1854. https://doi.org/10.1002/aic.690450902
- Meakin, P., & Tartakovsky, A. M. (2009). Modeling and simulation of pore-scale multiphase fluid flow and reactive transport in fractured and porous media. *Reviews of Geophysics*, 47, RG3002. https://doi.org/10.1029/2008rg000263
- Mostaghimi, P., Bijeljic, B., & Blunt, M. J. (2012). Simulation of flow and dispersion in pore-space images. SPE Journal, 17, 1131–1141. https://doi.org/10.2118/135261-pa
- Pini, R., Vandehey, N. T., Druhan, J., O'Neil, J. P., & Benson, S. M. (2016). Quantifying solute spreading and mixing in reservoir rocks using 3-D PET imaging. *Journal of Fluid Mechanics*. 796, 558–587. https://doi.org/10.1017/jfm.2016.262
- Raeini, A. Q., Blunt, M. J., & Bijeljic, B. (2014). Direct simulations of two-phase flow on micro-CT images of porous media and upscaling of pore-scale forces. Advances in Water Resources, 74, 116–126. https://doi.org/10.1016/j.advwatres.2014.08.012
- Risken, H. (1996). Fokker-planck equation (pp. 63-95): Springer. https://doi.org/10.1007/978-3-642-61544-3\_4
- Rizzo, C. B., & de Barros, F. P. J. (2017). Minimum hydraulic resistance and least resistance path in heterogeneous porous media. Water Resources Research. 53, 8596–8613. https://doi.org/10.1002/2017wr020418
- Rizzo, C. B., Nakano, A., & de Barros, F. P. J. (2019). PAR 2: Parallel random walk particle tracking method for solute transport in porous media. Computer Physics Communications, 222–239, 265–271. https://doi.org/10.1016/j.cpc.2019.01.013
- Sahimi, M. (2011). Flow and transport in porous media and fractured rock. (2nd ed.). Wiley. https://onlinelibrary.wiley.com/doi/book/10.1002/9783527636693
- Sahimi, M., Davis, H. T., & Scriven, L. E. (1983). Dispersion in disordered porous media. *Chemical Engineering Communications*, 23, 329–341. https://doi.org/10.1080/00986448308940483
- Sahimi, M., Heiba, A. A., Davis, H. T., & Scriven, L. E. (1986a). Dispersion in flow through porous media: II. Two-phase flow. Chemical Engineering Science, 41, 2123–2136. https://doi.org/10.1016/0009-2509(86)87129-9
- Sahimi, M., Hughes, B. D., Scriven, L. E., & Davis, H. T. (1986b). Dispersion in flow through porous media: I. One-phase flow. Chemical Engineering Science, 41, 2103–2122. https://doi.org/10.1016/0009-2509(86)87128-7
- Sahimi, M., & Imdakm, A. O. (1988). The effect of morphological disorder on hydrodynamic dispersion in flow through porous media. Journal of Physics A, 21, 3833–3870. https://doi.org/10.1088/0305-4470/21/19/019
- Salamon, P., Fernandez-Garcia, D., & Gómez-Hernández, J. J. (2006). A review and numerical assessment of the random walk particle tracking method. *Journal of Contaminant Hydrology*, 87, 277–305. https://doi.org/10.1016/j.jconhyd.2006.05.005
- Schmidhuber, J. (2014). Deep learning in neural networks: An overview. arXiv:1404.7828v4 [cs.NE] 8 Oct 2014.
- Shen, D., Wu, G., & Suk, H.-I. (2017). Deep learning in medical image analysis. *Annual Review of Biomedical Engineering*, 19, 221–248. https://doi.org/10.1146/annurev-bioeng-071516-044442
- Tahmasebi, P., Kamrava, S., Bai, T., & Sahimi, M. (2020). Machine learning in geo- and environmental sciences: From small to large scale. Advances in Water Resources, 142, 103619. https://doi.org/10.1016/j.advwatres.2020.103619
- Tahmasebi, P., Sahimi, M., Kohanpur, A. H., & Valocchi, A. J. (2017). Pore-scale simulation of flow of and brine in reconstructed and actual 3D rock cores. *Journal of Petroleum Science and Engineering*, 155, 21–33. https://doi.org/10.1016/j.petrol.2016.12.031
- Valvatne, P. H., & Blunt, M. J. (2004). Predictive pore-scale modeling of two-phase flow in mixed wet media. Water Resources Research, 40, W07406. https://doi.org/10.1029/2003wr002627
- Wu, H., Fang, W.-Z., Kang, Q., Tao, W.-Q., & Qiao, R. (2019). Predicting effective diffusivity of porous media from images by deep learning. Scientific Reports, 9, 20387. https://doi.org/10.1038/s41598-019-56309-x
- Zahasky, C., & Benson, S. M. (2018). Micro-positron emission tomography for measuring sub237 core scale single and multiphase transport parameters in porous media. *Advances in Water Resources*, 115, 1–16. https://doi.org/10.1016/j.advwatres.2018.03.002

KAMRAVA ET AL. 7 of 7